Mineralogical Magazine, December 2018, Vol. 82(6), pp. 1355–1367

The crystal-structure determination and redefinition of eztlite, $Pb_2^{2+}Fe_3^{3+}(Te^{4+}O_3)_3(SO_4)O_2Cl$

Owen P. Missen[1,2,*,‡], Stuart J. Mills[1], John Spratt[3], Mark D. Welch[4], William D. Birch[1], Michael S. Rumsey[4] and Jan Vylita[5]

[1] Geosciences, Museums Victoria, GPO Box 666, Melbourne 3001, Victoria, Australia
[2] School of Chemistry, University of Melbourne, Parkville 3010, Victoria, Australia
[3] Department of Core Research Laboratories, Natural History Museum, Cromwell Road, London SW7 5BD, England, UK
[4] Department of Earth Sciences, Natural History Museum, Cromwell Road, London SW7 5BD, England, UK
[5] Na Ostrohu 47, Praha 6, 16000, Czech Republic

[*Received 15 March 2018; Accepted 27 April 2018; Associate Editor: Ferdinando Bosi*]

ABSTRACT

The crystal structure of eztlite has been determined using single-crystal synchrotron X-ray diffraction and supported using electron microprobe analysis and powder diffraction. Eztlite, a secondary tellurium mineral from the Moctezuma mine, Mexico, is monoclinic, space group *Cm*, with $a = 11.466(2)$ Å, $b = 19.775(4)$ Å, $c = 10.497(2)$ Å, $\beta = 102.62(3)°$ and $V = 2322.6(9)$ Å^3. The chemical formula of eztlite has been revised to $Pb_2^{2+}Fe_3^{3+}(Te^{4+}O_3)_3(SO_4)O_2Cl$ from that stated previously as $Fe_6^{3+}Pb_2^{2+}(Te^{4+}O_3)_3(Te^{6+}O_6)(OH)_{10}{\cdot}nH_2O$. This change has been accepted by the Commission on New Minerals, Nomenclature and Classification of the International Mineralogical Association, Proposal 18-A. Eztlite was reported originally to be a mixed-valence Te oxysalt; however the crystal structure, bond-valence analysis and charge balance considerations clearly show that all Te is tetravalent. Eztlite contains a unique combination of elements and is only the second Te oxysalt to contain both sulfate and chloride. The crystal structure of eztlite contains mitridatite-like layers, with a repeating triangular nonameric $[Fe_9^{3+}O_{36}]^{45-}$ arrangement formed by nine edge-sharing $Fe^{3+}O_6$ octahedra, decorated by four trigonal pyramidal $Te^{4+}O_3$ groups, compared to PO_4 or AsO_4 tetrahedra in mitridatite-type minerals. In eztlite, all four tellurite groups associated with one nonamer are orientated with the lone pair of the Te atoms pointing in the same direction, whereas in mitridatite the central tetrahedron is orientated in the opposite direction to the others. In mitridatite-type structures, interlayer connections are formed exclusively *via* Ca^{2+} and water molecules, whereas the eztlite interlayer contains Pb^{2+}, sulfate tetrahedra and Cl^-. Interlayer connectivity in eztlite is achieved primarily by connections *via* the long bonds of $Pb\varphi_8$ and $Pb\varphi_9$ groups to sulfate tetrahedra and to Cl^-. Secondary connectivity is *via* Te–O and Te–Cl bonds.

Keywords: eztlite, crystal structure, tellurite, synchrotron radiation, tellurium oxysalt, mitridatite.

Introduction

The Moctezuma mine, Sonora, Mexico (29°48′N, 109°40′W), is the type locality for 21 Te oxysalt minerals, constituting approximately one quarter of all known secondary Te minerals (Christy *et al.*, 2016; Pasero *et al.*, 2017). This extraordinary mineralogical diversity was one of the driving forces behind increased study of Te that has occurred from the 1960s onwards. Despite this mineralogical diversity, a number of Te oxysalts first described at Moctezuma still have unknown crystal structures. The determination of these crystal structures will provide further information

*E-mail: omissen@museum.vic.gov.au
‡Present address: School of Earth, Atmosphere and Environment, Monash University, Clayton 3800, Victoria, Australia.
https://doi.org/10.1180/mgm.2018.108

about the formation of these minerals and their relationship to other Te oxysalts. The present investigation uses synchrotron X-ray diffraction, first used successfully on a secondary Te mineral in determining the structure of quetzalcoatlite (Burns *et al.*, 2000).

Eztlite was first reported as having the formula $Fe_6^{3+}Pb_2^{2+}(Te^{4+}O_3)_3(Te^{6+}O_6)(OH)_{10}\cdot nH_2O$, where $n \approx 8$ (Williams, 1982). It is one of six secondary Te minerals reported to contain both the +4 and +6 oxidation states of Te (Pasero *et al.*, 2017). However, of these species, only carlfriesite has a confirmed crystal structure that shows both oxidation states are indeed present (Effenberger *et al.*, 1978). The structures of 26 synthetic compounds with mixed Te oxidation states are known (Christy *et al.*, 2016), confirming that a greater variety in mixed-valence species than currently known in nature is possible.

This redefinition of eztlite follows on from other recent studies of existing secondary Te minerals (e.g. Christy *et al.*, 2016; Kampf *et al.*, 2017).

Specimen descriptions

Two eztlite specimens were analysed in this investigation. One was a type specimen (probably part of an original, single holotype) from the Moctezuma mine, registered in the collections of the Natural History Museum, London, specimen number BM 1984,468, which showed evidence of striations where a previous investigator had scraped away material for analysis. No obvious single crystals were observed, although eztlite was clearly present as blood-red crusts (Fig. 1*a*), surrounded by mixed Fe and Te oxides. A large number of small (<100 μm) aggregates of poughite are also found on this specimen.

A second eztlite specimen, which also originated from the Moctezuma mine, was recently purchased and is registered in the collections of Museums Victoria, registration number M54056. This specimen was used to obtain crystals of higher quality than were present on the type specimen, allowing for single-crystal analysis of eztlite to be performed. This specimen contains a cluster of sparkling, deep-red aggregates of prismatic eztlite crystals, on the surface of a rock otherwise rich in quartz, calcite and Fe oxides. Several spherical aggregates of emmonsite are also present. There are >100 eztlite aggregates covering an area of ~1 mm^2, with no eztlite obviously present on the rest of the specimen (see Fig. 1*b*). Iridescent

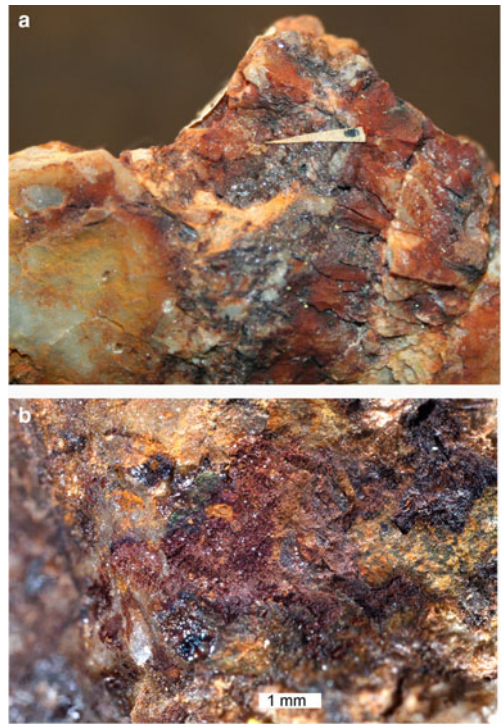

FIG. 1. (*a*) A view of the eztlite type specimen, BM 1984,468, showing red eztlite (a thin coating of poorly crystalline material next to the arrow), with orange, red and black iron–tellurium oxides on quartz. Several small aggregates of yellow poughite are also visible in the bottom half of the image. Field of view 3.5 mm. (*b*) A view of the M54056 specimen, showing dark red eztlite aggregates which are surrounded by Fe oxide films and other Fe oxides on quartz.

Fe-oxide films, powdery orange Fe oxides and botryoidal hematite surround the eztlite aggregates.

Chemistry

Quantitative chemical analyses of both eztlite specimens were performed on a Cameca SX100 Electron Microprobe in wavelength-dispersive mode, with an accelerating voltage of 12 kV, a specimen current of 10 nA, a beam diameter of 5 μm and PAP matrix correction (Pouchou and Pichoir, 1991) at the Imaging and Analysis Centre, Core Research Laboratories, Natural History Museum, London. The standards used for each element were: baryte (S), halite (Cl), wollastonite (Ca), hematite (Fe), sphalerite (Zn), TeO_2 (Te) and vanadinite (Pb). The sample was assumed to contain significant OH

TABLE 1. Electron microprobe data for the two eztlite specimens, including the analysis by Williams (1982) for comparison.

	Type specimen (BM 1984,468) 17 analyses				M54056 specimen 10 analyses				Williams (1982)
Oxide wt.%	Avg	Min	Max	S.D.	Avg	Min	Max	S.D.	Average
SO_3	6.20	6.02	6.32	0.10	6.22	6.04	6.39	0.12	n.k.
Cl	2.64	2.41	2.85	0.13	2.68	2.52	2.78	0.08	n.k.
CaO	0.15	0.00	0.21	0.05	0.14	0.07	0.18	0.03	n.k.
Fe_2O_3	18.9	18.5	19.4	0.22	18.7	18.4	18.9	0.17	24.3
ZnO	bdl	bdl	bdl	bdl	0.18	0.00	0.36	0.15	n.k.
TeO_2	37.9	37.4	38.9	0.30	37.1	36.4	37.7	0.43	26.8
TeO_3*	–	–	–	–	–	–	–	–	8.6
PbO	34.1	33.4	34.7	0.34	34.2	33.6	34.7	0.35	25.5
H_2O*	–	–	–	–	–	–	–	–	12.3
O=Cl	–0.60				–0.61				–
Total	99.25				98.60				97.5

* TeO_3 and H_2O were only detected by Williams and are not actually present in eztlite.
S.D. – standard deviation; bdl – below detection limit; n.k. – not known

TABLE 2. Powder X-ray diffraction data for eztlite to 45°2θ.

I_{obs}	d_{obs}	d_{calc}	I_{calc}	$h\ k\ l$
10	10.299	10.243	54	0 0 1
11	5.695	5.679	27	1 3 0
18	5.596	5.594	45	2 2 0
12	5.236	5.219	30	$\bar{1}$ 3 1
17	5.136	5.121	44	0 0 2
16	4.745	4.749	48	1 3 1
11	4.518	5.513	23	2 0 1
11	4.290	4.271	27	$\bar{2}$ 0 2
45	4.038	4.032	100	$\bar{1}$ 3 2
17	3.724	3.729	15	1 5 0
55	3.422	3.414	85	0 0 3
100	3.291	3.296	73	0 6 0
		3.279	93	$\bar{3}$ 3 1
		3.246	32	3 3 0
73	3.241	3.237	38	3 1 1
		3.232	45	$\bar{2}$ 4 2
25	3.135	3.125	36	$\bar{1}$ 5 2
31	3.018	3.013	49	$\bar{3}$ 3 2
42	2.943	2.938	65	3 3 1
15	2.823	2.818	16	$\bar{2}$ 6 1
26	2.801	2.797	14	4 0 0
		2.793	25	1 3 3
27	2.779	2.772	44	0 6 2
34	2.667	2.667	26	2 0 3
		2.662	31	2 6 1
49	2.616	2.609	48	$\bar{2}$ 6 2
31	2.566	2.561	21	0 0 4
		2.560	17	4 0 1
46	2.447	2.441	11	$\bar{4}$ 0 3
		2.428	49	$\bar{1}$ 3 4
29	2.377	2.374	12	$\bar{4}$ 2 3
		2.371	19	1 1 4
22	2.353	2.349	13	$\bar{3}$ 1 4
		2.347	17	2 4 3
19	2.283	2.278	15	$\bar{5}$ 1 1
27	2.266	2.263	15	$\bar{3}$ 7 1
22	2.232	2.227	25	$\bar{3}$ 3 4
20	2.160	2.157	20	3 3 3

Only I_{calc} >15% are shown.

(Williams, 1982) so low values of voltage and current were used to reduce expected dehydration during analysis. Consequently, results are recorded to only one decimal place for Fe, Te and Pb. These beam conditions input less energy into the sample but give lower counting statistics for determined elements. Analytical results (Table 1) for the two samples are near identical, with both containing essential Pb^{2+}, Fe^{3+}, Te^{4+}, S and Cl. M54056 contains minor Zn, and both specimens contain minor Ca. No other elements were detected using

TABLE 3. Crystallographic information relating to data collection and refinement of eztlite.

Crystal data	
Ideal chemical formula	$Pb_2^{2+}Fe_3^{3+}(Te^{4+}O_3)_3(SO_4)O_2Cl$
Crystal system, space group	Monoclinic, *Cm*
Temperature (K)	100(2)
a, *b*, *c* (Å)	11.466(2), 19.775(4), 10.497(2)
α, β, γ (°)	90, 102.62(3), 90
V (Å^3)	2322.6(9)
Z	2
Calculated density (g cm^{-3})	5.458
Radiation type and wavelength (Å)	Synchrotron, λ = 0.71073
μ (mm^{-1})	30.340
Crystal dimensions (mm)	0.004 × 0.005 × 0.005
Reflections for cell refinement	21,811
Data Collection	
Crystal description	Pale red fragment
Diffractometer	Dectris EigerX 16M
θ (°) range	1.988, 32.365
Index ranges	$-16 \le h \le 16$, $-29 \le k \le 29$, $-15 \le l \le 15$
Absorption correction	Multi-scan *SADABS* (Bruker, 2001)
T_{max} , T_{min}	0.3354, 0.4346
No. of measured, independent and observed [$I > 2\sigma(I)$] reflections	20,859, 7016, 6519
R_{int}	0.0496
Data completeness to 25.242°θ (%)	99.4%
Refinement	
Number of reflections, parameters, restraints	7016, 364, 2
$R_1[F^2 > 2\sigma(F^2)]$, R_1(all)	0.0360, 0.0392
$wR_2[F^2 > 2\sigma(F^2)]$, wR_2(all)	0.0877, 0.0890
GoF (F^2)	1.023
$\Delta\rho_{max}$, $\Delta\rho_{min}$ (e^- Å^{-3})	3.63, –3.91

energy-dispersive spectroscopy or the electron microprobe. There was insufficient eztlite for CHN or infrared analyses. Raman spectroscopy was attempted, but excessive fluorescence prevented meaningful results from being obtained. Thus the crystal-structure analysis (see below) was used to show that eztlite is anhydrous.

The chemical analysis of eztlite yields an unambiguous elemental composition that is significantly different to that reported by Williams (1982). The empirical formula (based on 15O anions per formula unit) for the type specimen is $Pb_{1.94}Ca_{0.03}Fe_{3.01}Te_{3.02}S_{0.99}Cl_{0.95}O_{15.00}$ and for M54056 is $Pb_{1.97}Ca_{0.03}Zn_{0.03}Fe_{3.01}Te_{2.98}S_{1.00}Cl_{0.97}O_{15.00}$. Both formulae may be approximated as $Pb_2^{2+}Fe_3^{3+}Te_3^{4+}SClO_{15}$. As all Te^{4+} centres are in trigonal pyramidal geometry (see below), the end-member formula of eztlite is $Pb_2^{2+}Fe_3^{3+}(Te^{4+}O_3)_3(SO_4)O_2Cl$, which requires PbO 34.75%, Fe_2O_3 18.99%, TeO_2 37.27%, SO_3 6.23%, Cl 2.76%, total 100 wt.%.

Compared to Williams (1982), the analyses of type eztlite (BM 1984,468) contain significantly lower Fe_2O_3 (18.89% compared to 24.3%), significantly higher PbO (34.10% compared to 25.5%) and similar overall Te (37.87% TeO_2 compared to 26.8% TeO_2 and 8.6% TeO_3). Williams (1982) and his analyst, Marjorie Duggan, analysed for Al, Mn, Fe, Te (both valences) and Pb by wet chemical methods when determining the chemical composition of eztlite. No mention is made of analysing for S or Cl. The lack of these two elements yields an ideal mass deficit (SO_3 + Cl) of 8.99 wt.%, which corresponds roughly to the 12.3 wt% H_2O determined by the Penfield method on a 945 μg sample of 'eztlite' (Williams, 1982). Presumably the Penfield analysis incorporated some hydrous material along with eztlite, or analysed a hydrous phase instead of eztlite, as eztlite is now known to be anhydrous. The presence of a second phase is also a possible source of the

TABLE 4. Bond lengths (Å) for eztlite*.

Pb1–O14	2.474(12)	Te1–O4	1.866(16)	Fe1–O6	1.929(10)
Pb1–O26	2.566(16)	Te1–O16 (×2)	1.884(10)	Fe1–O9	1.982(11)
Pb1–O7	2.576(11)	Te1–O2 (×2)	3.130(11)	Fe1–O14	2.025(13)
Pb1–O17	2.589(12)	Te1–O8 (×2)	3.154(12)	Fe1–O5	2.047(11)
Pb1–O18	2.617(12)	Te1–O11 (×2)	3.204(11)	Fe1–O3	2.058(11)
Pb1–Cl1	2.855(7)	<Te1–O>	2.734	Fe1–O7	2.075(11)
Pb1–O22	2.873(15)			<Fe1–O>	2.019
Pb1–O21	2.992(7)	Te2–O1	1.882(11)		
Pb1–O25	3.31(2)	Te2–O5	1.884(12)	Fe2–O10	1.938(16)
<Pb1–φ>	2.761	Te2–O3	1.884(10)	Fe2–O13	1.962(18)
		Te2–O18	2.992(12)	Fe2–O19	1.988(19)
Pb2–O11 (×2)	2.451(11)	Te2–O17	3.063(12)	Fe2–O1 (×2)	2.059(11)
Pb2–O20	2.49(2)	Te2–O15	3.066(12)	Fe2–O12	2.083(15)
Pb2–O13	2.564(17)	<Te2–O>	2.462	<Fe2–O>	2.015
Pb2–O10	2.651(14)				
Pb2–O25 (×2)	2.775(19)	Te3–O15	1.891(11)	Fe3–O7	1.937(11)
Pb2–O21	3.21(2)	Te3–O14	1.891(11)	Fe3–O2	1.993(12)
<Pb2–O>	2.671	Te3–O18	1.898(12)	Fe3–O18	2.004(12)
		Te3–O22	3.040(13)	Fe3–O6	2.023(11)
Pb3–O9	2.484(11)	Te3–O26	3.176(18)	Fe3–O16	2.053(10)
Pb3–O8	2.542(11)	Te3–O6	3.310(9)	Fe3–O3	2.065(10)
Pb3–O2	2.590(12)	Te3–Cl1	3.512(7)	<Fe3–O>	2.013
Pb3–O24	2.630(15)	Te3–Cl1	3.535(9)		
Pb3–O6	2.664(9)	<Te3–φ>	2.782	Fe4–O7	1.920(11)
Pb3–O23	2.716(18)			Fe4–O17	1.995(12)
Pb3–Cl2	2.878(8)	Te4–O19	1.871(17)	Fe4–O11	2.005(11)
Pb3–Cl1	2.979(6)	Te4–O17 (×2)	1.893(11)	Fe4–O10	2.009(10)
<Pb3–φ>	2.685	Te4–O21	3.04(2)	Fe4–O4	2.064(11)
		Te4–O10	3.318(14)	Fe4–O5	2.076(10)
Pb4–O12	2.480(16)	<Te4–O>	2.403	<Fe4–O>	2.012
Pb4–O15 (×2)	2.549(11)				
Pb4–O19	2.592(19)	Te5–O13	1.862(17)	Fe5–O12	1.942(5)
Pb4–O22 (×2)	2.877(15)	Te5–O8 (×2)	1.892(10)	Fe5–O8	1.993(12)
Pb4–Cl2 (×2)	3.003(7)	Te5–O23	2.943(17)	Fe5–O6	2.001(9)
<Pb4–φ>	2.741	Te5–O23	2.943(16)	Fe5–O15	2.034(12)
		Te5–O12	3.351(16)	Fe5–O1	2.056(11)
S1–O22 (×2)	1.484(13)	Te5–Cl2	3.425(10)	Fe5–O16	2.061(11)
S1–O20	1.50 (2)	Te5–Cl2	3.425(9)	<Fe5–O>	2.015
S1–O21	1.50(2)	<Te5–φ>	2.717		
<S1–O>	1.492				
		Te6–O9	1.861(11)		
S2–O25	1.483(18)	Te6–O2	1.875(11)		
S2–O24	1.500(18)	Te6–O11	1.906(11)		
S2–O26	1.503(15)	Te6–O24	2.940(14)		
S2–O23	1.520(18)	Te6–O25	2.962(18)		
<S2–O>	1.502	Te6–O20	3.330(11)		
		Te6–O7	3.377(11)		
		<Te6–O>	2.607		

*For Te and Pb, φ denotes average bond length incorporating both O and Cl.

TABLE 5. Bond-valence sums (in valence units, vu) for eztlite.

Atom	Pb1	Pb2	Pb3	Pb4	Te1	Te2	Te3	Te4	Te5	Te6	Fe1	Fe2	Fe3	Fe4	Fe5	S1	S2	Σ
Cl1	0.415		0.297				0.110; 0.115											**0.938**
Cl2			0.390	0.278 (×2↓)					0.134 (×2↓)									**0.803**
O1						1.211						0.443 (×2↓)			0.447			**2.101**
O2			0.278		0.058 (×2↓)					1.232			0.532					**2.100**
O3						1.205					0.444		0.436					**2.085**
O4					1.259									0.437 (×2→)				**2.133**
O5						1.205					0.458			0.423				**2.086**
O6			0.239				0.037				0.636		0.490		0.521			**1.923**
O7	0.286									0.032	0.424		0.622	0.652				**2.016**
O8			0.307		0.054 (×2↓)				1.182 (×2↓)						0.532			**2.075**
O9			0.345							1.275	0.549							**2.169**
O10		0.246						0.036				0.620		0.509 (×2→)				**1.921**
O11		0.369 (×2↓)			0.048 (×2↓)					1.142				0.515				**2.075**
O12				0.348					0.034			0.415 (×2→)			0.613			**2.023**
O13		0.293							1.272			0.580						**2.145**
O14	0.352						1.185				0.487							**2.024**
O15				0.302 (×2↓)		0.067	1.185								0.475			**2.030**
O16					1.205 (×2↓)								0.451		0.441			**2.096**
O17	0.279					0.068		1.179 (×2↓)						0.529				**2.055**
O18	0.263					0.081	1.165						0.516					**2.025**
O19				0.277				1.244				0.540						**2.061**
O20		0.341								0.035 (×2→)						1.399		**1.811**
O21	0.122 (×2→)	0.078						0.072								1.399		**1.794**
O22	0.156			0.155 (×2↓)			0.072									1.456 (×2↓)		**1.839**
O23			0.215						0.091 (×2↓)								1.331	**1.637**
O24			0.256							0.092							1.399	**1.747**
O25	0.064	0.191 (×2↓)								0.087							1.460	**1.802**
O26	0.292						0.052										1.389	**1.732**
Σ	**2.231**	**2.079**	**2.328**	**2.097**	**3.990**	**3.837**	**3.933**	**3.710**	**4.120**	**3.894**	2.998	**3.041**	**3.047**	**3.065**	**3.029**	**5.711**	**5.578**	

erroneous presence of Te^{6+} that Williams (1982) determined in eztlite.

Crystallography

Powder diffraction

An eztlite aggregate comprising eleven sub-spherical eztlite grains obtained from the type specimen (BM 1984,468) was attached to a non-diffracting amorphous-carbon fibre (10 μm diameter) that was glued to a glass support rod. This sample was mounted on a Rigaku R-Axis curved image-plate diffractometer (®Rigaku Oxford Diffraction) at the Natural History Museum (London), and a dataset collected using Cu*K*α radiation. A Gandolfi-type randomized sample movement was achieved by rotations on the φ and ω axes. Observed d_{hkl} and reflection intensities collected to $2\theta = 90°$ were derived by profile-fitting using *Highscore Plus* software (Degen *et al.*, 2014), although the dataset used was truncated at $2\theta = 60°$ due to poorly defined, low-intensity peaks at higher angles. High background resulted in lower than expected relative intensities for peaks at low values of 2θ. The intensities of calculated and observed patterns commonly showed discrepancies, although this is not unexpected as the maximum intensity peak was different for the observed and calculated patterns. Nonetheless, the *d* values were mostly in good agreement.

The unit-cell parameters of eztlite were refined using *Chekcell* (Laugier and Bochu, 2004) from the powder data and are $a = 11.468(2)$ Å, $b = 19.769(3)$ Å, $c = 10.510(2)$ Å, $\beta = 102.74(1)°$ and $V = 2324.0(3)$ Å^3. These parameters are in good agreement with the synchrotron single-crystal unit cell and with the pattern calculated from the structure using the *PowderCell* program (Kraus and Nolze, 1996). This result confirms that the material analysed on the type specimen is identical to that on M54056. A comparison of observed and calculated peaks for the powder diffraction data is given in Table 2. Although the powder lines collected by Williams (1982) match peaks observed in this study, showing that the powder pattern he collected was from pure eztlite, he indexed a different monoclinic cell with the unit-cell parameters $a = 6.58$, $b = 9.68$, $c = 20.52$ Å, $\beta = 90.25°$ and $V = 1307$ Å^3.

Single-crystal diffraction

The single-crystal X-ray diffraction experiment was carried out on the micro-focus macromolecular MX2 beamline at the Australian Synchrotron, part of ANSTO. A 4 μm × 4 μm × 5 μm pale-red single crystal of eztlite was selected from specimen M54056. Data were collected at 100 K by a Dectris EigerX 16M detector using monochromatic radiation with a wavelength of 0.71073 Å. Further details of data collection and structure refinement are provided in Table 3.

After processing the data using *XDS* (Kabsch, 2010), *XPREP* (Bruker, 2001) and *SADABS* (Bruker, 2001), 20,859 reflections were found with an R_{int} of 0.0496. Structure solution in space group *Cm* was carried out by direct methods using *SHELXT* (Sheldrick, 2015*a*) and four Pb, six Te, five Fe, two S, one Cl and 27 O atoms were located. Structure refinement by full-matrix least-squares was implemented by *SHELXL* (Sheldrick, 2015*b*), using neutral atomic-scattering factors. The final structure contains two Cl and 26 O atoms as one of the 'oxygen' atoms was determined to be a Cl site. All atom positions and anisotropic displacement parameters (U^{ij}) were refined to final R_1 and wR_2 values of 0.0360 and 0.0877, respectively. After refining until the weighting scheme converged, and omitting all reflections with calculated F_0/F_C errors greater than 5.00, one atom (O16) remained as non-positive definite. This is attributed to the position of O16 at an apex site in the mitridatite-like layers (see next section), which is postulated to cause the observed distortion. Despite this, all bond lengths to O16 are chemically sensible (Table 4). A summary of bond valences is provided in Table 5, using the parameters of Brese and O'Keefe (1991) for Pb–Cl bonds, Krivovichev and Brown (2001) for Pb–O bonds, Mills and Christy (2013) for Te^{4+}–O and Te^{4+}–Cl bonds, and the parameters of Gagné and Hawthorne (2015) for Fe^{3+}–O and S–O bonds. Fractional atom coordinates, site occupancies and atom displacement parameters (U^{ij}) for all atoms are shown in Table 6.

The crystallographic files have been deposited with the Principal Editor of *Mineralogical Magazine* and are available as Supplementary material (see below).

Crystal-structure description

The crystal structure of eztlite is best described as a complex layered arrangement, with layers formed from $Fe^{3+}O_6$ octahedra and $Te^{4+}O_3$ trigonal pyramids. This arrangement is pseudo-trigonal, however other, less-ordered components in the structure result in a monoclinic habit overall.

TABLE 6. Fractional atom coordinates, occupancies and displacement parameters for the atomic sites of eztlite.

Atom	*x/a*	*y/b*	*z/c*	Occ	U_{eq}	U^{11}	U^{22}	U^{33}	U^{23}	U^{13}	U^{12}
Pb1	0.84063(5)	0.85743(3)	0.10740(6)	1	0.01866(12)	0.0155(3)	0.0144(2)	0.0277(3)	0.0018(2)	0.0084(2)	0.0009(2)
Pb2	0.24430(7)	½	0.69945(8)	1	0.01829(16)	0.0152(3)	0.0176(4)	0.0237(4)	0	0.0078(3)	0
Pb3	0.28460(6)	0.81719(3)	0.70074(6)	1	0.02516(15)	0.0316(3)	0.0166(3)	0.0287(3)	−0.0006(2)	0.0094(3)	0.0055(2)
Pb4	0.76100(11)	½	0.11591(10)	1	0.0290(2)	0.0445(6)	0.0165(4)	0.0270(4)	0	0.0102(4)	0
Te1	0.55817(12)	½	0.47256(13)	1	0.0137(2)	0.0119(5)	0.0095(5)	0.0212(6)	0	0.0071(5)	0
Te2	0.52463(9)	0.83267(5)	0.30840(10)	1	0.01521(18)	0.0130(4)	0.0098(4)	0.0245(4)	0.0003(3)	0.0074(3)	−0.0004(3)
Te3	0.67213(9)	0.68887(5)	0.11770(9)	1	0.01432(18)	0.0146(4)	0.0103(4)	0.0192(4)	−0.0005(3)	0.0064(3)	−0.0003(3)
Te4	0.10965(12)	½	0.11710(13)	1	0.0157(2)	0.0137(6)	0.0144(6)	0.0203(6)	0	0.0063(5)	0
Te5	0.89737(13)	½	0.68452(13)	1	0.0161(2)	0.0132(6)	0.0167(6)	0.0190(6)	0	0.0047(5)	0
Te6	0.45145(9)	0.64745(5)	0.68838(9)	1	0.01505(18)	0.0164(4)	0.0104(4)	0.0195(4)	−0.0002(3)	0.0065(4)	0.0009(3)
Fe1	0.8121(2)	0.76824(11)	0.4079(2)	1	0.0122(3)	0.0105(8)	0.0076(7)	0.0202(9)	−0.0001(7)	0.0069(7)	−0.0005(7)
Fe2	0.0083(3)	½	0.4049(3)	1	0.0131(5)	0.0106(12)	0.0081(11)	0.0229(14)	0	0.0087(10)	0
Fe3	0.55765(19)	0.66765(11)	0.4022(2)	1	0.0136(4)	0.0107(9)	0.0073(8)	0.0244(10)	−0.0001(7)	0.0073(8)	0.0003(7)
Fe4	0.2831(2)	0.57631(10)	0.4001(2)	1	0.0130(4)	0.0118(9)	0.0072(8)	0.0219(9)	0.0006(7)	0.0079(7)	−0.0001(7)
Fe5	0.78740(19)	0.59213(11)	0.4015(2)	1	0.0132(4)	0.0108(9)	0.0086(8)	0.0217(9)	−0.0003(7)	0.0067(7)	−0.0004(7)
S1	0.4596(5)	½	0.9864(6)	1	0.0187(10)	0.017(2)	0.017(2)	0.023(3)	0	0.006(2)	0
S2	0.1266(5)	0.6686(2)	0.8152(5)	1	0.0301(9)	0.029(2)	0.026(2)	0.038(3)	0.0046(18)	0.0116(19)	0.0041(18)
Cl1	0.8939(7)	0.7461(4)	−0.0435(7)	0.75	0.0427(18)	0.032(3)	0.056(4)	0.037(3)	−0.025(3)	0.001(3)	0.009(3)
Cl2	0.2222(9)	0.9213(5)	0.8655(8)	0.75	0.054(2)	0.066(6)	0.051(5)	0.050(4)	−0.022(4)	0.027(4)	−0.008(4)
O1	0.4673(10)	0.8987(5)	0.4084(13)	1	0.020(2)	0.008(4)	0.008(4)	0.047(7)	−0.004(4)	0.011(5)	0.001(4)
O2	0.5696(10)	0.6460(6)	0.5900(11)	1	0.017(2)	0.013(5)	0.020(5)	0.019(5)	0.001(4)	0.009(4)	0.001(4)
O3	0.4844(10)	0.7624(5)	0.4121(11)	1	0.0146(19)	0.014(5)	0.005(4)	0.030(5)	0.000(4)	0.016(4)	−0.001(4)
O4	0.4000(14)	½	0.3785(15)	1	0.015(3)	0.017(7)	0.010(6)	0.019(7)	0	0.009(6)	0
O5	0.6810(10)	0.8381(5)	0.4114(12)	1	0.017(2)	0.014(5)	0.005(4)	0.033(6)	−0.003(4)	0.006(4)	−0.004(4)
O6	0.7358(10)	0.6850(5)	0.4407(9)	1	0.0106(18)	0.015(5)	0.006(4)	0.011(4)	−0.003(3)	0.005(4)	0.002(3)
O7	0.3899(10)	0.6436(5)	0.3588(11)	1	0.015(2)	0.010(4)	0.013(5)	0.024(5)	0.001(4)	0.009(4)	−0.003(4)
O8	0.8051(10)	0.5704(5)	0.5902(11)	1	0.016(2)	0.015(5)	0.010(4)	0.025(5)	−0.001(4)	0.006(4)	0.008(4)
O9	0.3630(11)	0.7185(5)	0.5992(11)	1	0.017(2)	0.024(6)	0.008(4)	0.020(5)	0.001(4)	0.008(4)	0.004(4)
O10	0.1815(14)	½	0.4410(14)	1	0.014(3)	0.018(7)	0.013(6)	0.011(6)	0	0.006(5)	0
O11	0.3597(10)	0.5768(5)	0.5910(11)	1	0.015(2)	0.017(5)	0.011(4)	0.018(5)	0.004(4)	0.005(4)	−0.001(4)
O12	0.8221(13)	½	0.3576(15)	1	0.013(3)	0.007(6)	0.008(6)	0.028(7)	0	0.010(6)	0
O13	1.0203(15)	½	0.5943(17)	1	0.023(3)	0.015(7)	0.026(8)	0.030(9)	0	0.008(7)	0
O14	0.7642(12)	0.7595(6)	0.2112(12)	1	0.024(3)	0.032(7)	0.014(5)	0.026(6)	−0.003(4)	0.004(5)	−0.012(5)
O15	0.7665(10)	0.6189(5)	0.2107(11)	1	0.016(2)	0.017(5)	0.010(4)	0.023(5)	0.002(4)	0.009(4)	0.003(4)
O16	0.6081(9)	0.5700(5)	0.3751(10)	1	0.0134(19)	0.014(5)	0.003(4)	0.025(5)	0.001(3)	0.010(4)	−0.006(4)
O17	0.1974(11)	0.5715(6)	0.2132(12)	1	0.021(2)	0.025(6)	0.009(5)	0.029(6)	−0.006(4)	0.008(5)	0.000(4)

O18	0.5510(10)	0.6916(6)	0.2153(12)	1	0.018(2)	0.015(5)	0.015(5)	0.024(5)	0.009(4)	0.006(4)	0.002(4)	
O19	−0.0107(16)	½	0.2121(19)	1	0.039(6)	0.009(7)	0.084(18)	0.029(9)	0	0.013(7)	0	
O20	0.4491(19)	½	0.841(2)	1	0.038(5)	0.022(9)	0.053(13)	0.034(10)	0	−0.005(8)	0	
O21	0.3360(17)	½	1.011(2)	1	0.031(4)	0.015(8)	0.041(11)	0.036(10)	0	0.007(7)	0	
O22	0.5273(13)	0.5603(7)	1.0458(13)	1	0.031(3)	0.032(7)	0.025(6)	0.036(7)	−0.010(5)	0.008(6)	−0.009(6)	
O23	0.0101(16)	0.6319(8)	0.7600(16)	1	0.042(4)	0.043(9)	0.035(8)	0.048(9)	−0.006(7)	0.010(7)	−0.002(7)	
O24	0.1194(13)	0.7397(8)	0.7636(15)	1	0.035(3)	0.028(7)	0.038(8)	0.041(8)	0.021(6)	0.009(6)	0.010(6)	
O25	0.2311(17)	0.6312(9)	0.789(2)	1	0.054(5)	0.041(10)	0.031(8)	0.101(15)	0.012(9)	0.037(10)	0.010(7)	
O26	0.1378(14)	0.6728(9)	0.9601(17)	1	0.040(4)	0.031(8)	0.041(9)	0.046(9)	0.012(7)	0.007(7)	−0.003(7)	

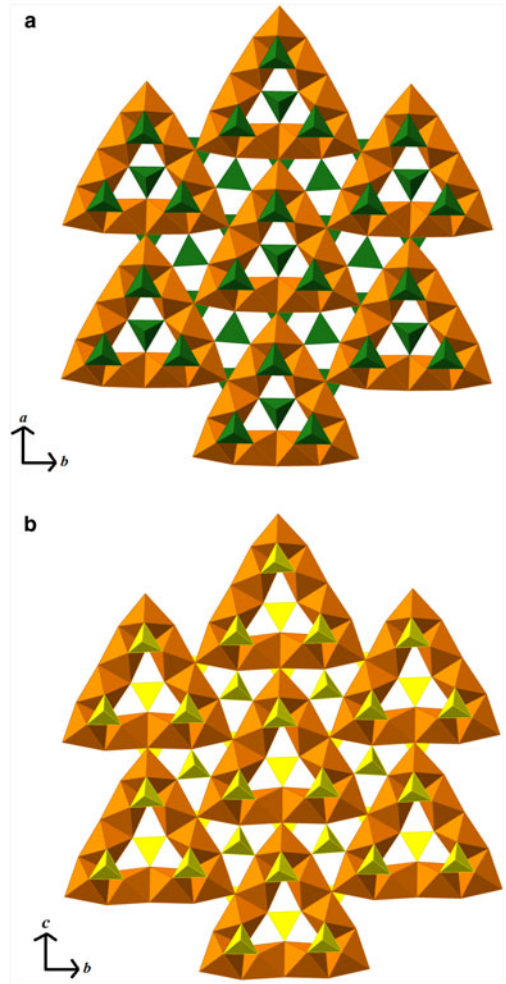

FIG. 2. (*a*) Eztlite layer, comprising $Fe^{3+}O_6$ octahedra in orange and $Te^{4+}O_3$ trigonal pyramids in dark green. Note that the tellurium atoms are orientated closest to the viewer in the centre of each nonameric unit. (*b*) Mitridatite layer, comprising $Fe^{3+}O_6$ octahedra in orange and PO_4 tetrahedra in yellow. Note that the phosphorus atoms in the centre of the nonameric units are orientated into the page. (Note that mitridatite was defined along different axes to eztlite; *a* swapped with *c*)

The interlayer regions are occupied by 8- and 9-coordinate Pb cations, sulfate tetrahedra, and chloride anions coordinated chiefly with Pb.

The layers in eztlite (see Fig. 2*a*) are analogous to the layers formed in mitridatite-type structures (see Fig. 2*b*). Mitridatite is a secondary Ca–Fe–phosphate mineral with the formula $Ca_2Fe^{3+}_3(PO_4)_3O_2{\cdot}3H_2O$ (Moore and Araki, 1977; Huminicki and Hawthorne, 2002). The other three group members

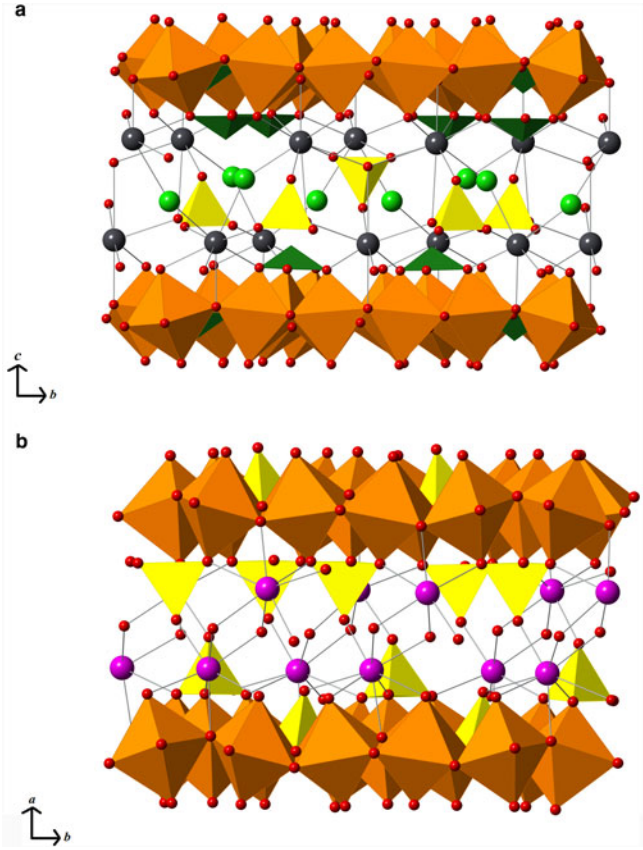

FIG. 3. (*a*) Two eztlite layers showing interlayer species ($Fe^{3+}O_6$ in orange and $Te^{4+}O_3$ in dark green). Pb^{2+} cations are shown in dark grey and Cl atoms in lime-green. Sulfate tetrahedra are shown in yellow (not to be confused with yellow phosphate tetrahedra in mitridatite). Oxygen atoms are shown as small red spheres. (*b*) Two mitridatite layers showing interlayer species ($Fe^{3+}O_6$ in orange). Yellow phosphate tetrahedra extend further into the layers than do the tellurite trigonal pyramids in eztlite. Ca^{2+} cations are in magenta. Non-bonded interstitial water molecules omitted for clarity. (Note that mitridatite was defined along different axes to eztlite.)

are arseniosiderite, the As analogue (Moore and Ito, 1974); kolfanite, the dihydrate (Voloshin *et al.*, 1982); and robertsite, the Mn^{3+} analogue (Andrade *et al.*, 2012). None of these minerals contain Pb, sulfate or chloride, instead containing interlayer water and Ca cations. In eztlite, the arrangement of nonameric triangles formed from edge-sharing $Fe^{3+}O_6$ octahedra, each of which in isolation has the formula $[Fe^{3+}_9O_{36}]^{45-}$ and which are linked to three adjacent triangles through corner-sharing at the central vertices of each side, is identical to that found in mitridatite. $Te^{4+}O_3$ trigonal pyramids decorate the triangular arrangement of $Fe^{3+}O_6$ octahedra, with four $Te^{4+}O_3$ groups associated directly with each nonamer (see Fig. 2*a*). The incorporation of tellurite polyhedra into the two-dimensional layers results in the empirical layer formula of $[Fe^{3+}(Te^{4+}O_3)O]^{1-}$. Mitridatite-type structures contain either PO_4 or AsO_4 tetrahedra, hence the three-coordinate Te deviates somewhat from mitridatite, though tellurite groups are found in similar crystallographic locations to the phosphate and arsenate in mitridatite (see Fig. 2*b*). Another difference between the structure types is that in mitridatite-type structures, the central tetrahedron points in the opposite direction to the three others, whereas in eztlite, all four of the $Te^{4+}O_3$ groups are orientated in the same direction with respect to the Te atom position. Eztlite crystallizes in *Cm*, which is a maximal subgroup of *Cc*, the space group in which mitridatite crystallizes.

Pb^{2+} cations are found above and below each mitridatite-like layer, bonding to oxygen atoms

TABLE 7. Summary of tellurium bonding in eztlite with bond lengths (Å) and bond valences (vu).

Te centre number	Te centre formula	<Te–O> primary bond length	<Te–O> primary bond valence	Number of secondary bonds	<Te–φ> secondary bond length	<Te–φ> secondary bond valence	Overall <Te–φ> bond length	Overall <Te–φ> bond valence
Te1	$Te^{4+}O_9$	1.878	3.669	6	3.163	0.321	2.734	3.990
Te2	$Te^{4+}O_6$	1.883	3.621	3	3.040	0.216	2.462	3.837
Te3	$Te^{4+}O_6Cl_2$	1.893	3.534	5	3.315	0.386	2.782	3.920
Te4	$Te^{4+}O_5$	1.886	3.602	2	3.179	0.108	2.403	3.710
Te5	$Te^{4+}O_6Cl_2$	1.882	3.635	5	3.217	0.485	2.717	4.120
Te6	$Te^{4+}O_7$	1.881	3.649	4	3.152	0.246	2.607	3.894
Average	$Te^{4+}O_{6.50}Cl_{0.67}$	1.884	3.618	4.17	3.178	0.294	2.617	3.912

both in the layers and at the vertices of the sulfate tetrahedra, and also to chloride ions (see Fig. 3*a*). The sulfate tetrahedra and chloride ions are found between the layers of lead cations. One third of the sulfate tetrahedra are oriented in the opposite direction to the others and the chloride ions are close to equidistant from both layers. This is in contrast to mitridatite-type structures, in which calcium and water fill the interstitial space (see Fig. 3*b*). Each of the four lead atoms in eztlite is found in a different coordination environment, in over-bonded environments with an average Pb bond-valence sum of 2.184 valence units (vu). Pb2 and Pb4 are in asymmetric configuration due to the stereoactive $6s^2$ lone pair, but Pb1 and Pb3 do not display obvious asymmetry. Pb1 is in 9-fold coordination (PbO_8Cl), while the other three are in 8-fold coordination: Pb2 as PbO_8 and Pb3 and Pb4 as PbO_6Cl_2.

It is also worth further examining the bonding of the Te atoms (see Table 7 for a Te bonding summary). Although each Te possesses three short, primary bonds to allow for the formation of the $Te^{4+}O_3$ trigonal pyramids, the average bond-valence sum for Te incorporating only primary bonds is 3.618 vu, indicating that the remaining valence of the Te cations is filled with longer secondary bonds to both oxygen and chlorine atoms. Tellurium secondary bonds thus play an important role in increasing the stability of the eztlite structure by providing crosslinks between the mitridatite-like layer and interstitial species. The majority, but not all, of these secondary bonds are on the same side of the Te atom as the lone pair. The number of secondary bonds varies between 2 and 6, with an average of 4.17 secondary bonds per Te atom, which fits well with the range observed by Christy and Mills (2013). Bond-valence sums for Te vary between 3.710 vu for Te4 (which is under-bonded due to only having two secondary linkages) to 4.120 vu for Te5, with an average bond valence of 3.912 vu, which is an average increase of 0.294 vu per Te atom once secondary bonds are incorporated. The Te3 and Te5 cations have the greatest proportion of their bond valence made up by secondary bonding as both of these Te centres have two Te–Cl secondary bonds which contribute more than 0.1 vu each.

Relationship to other Te oxysalt structures

Eztlite contains isolated *neso* tellurite $(Te^{4+}O_3)^{2-}$ groups that are part of a larger structural group (a layer based on edge and corner linking of $Fe^{3+}O_6$ octahedra, with tellurite decoration, in this case). The minerals juabite (Roberts *et al.*, 1997; Kampf

and Mills, 2011) and rodalquilarite (Feger *et al.*, 1999; Kampf and Mills, 2011) are also in this category, but display no structural similarities to eztlite (Christy *et al.*, 2016). Although also containing Te^{4+}, sulfate and chloride in a layered structure, nabokoite is markedly different to eztlite. All octahedral Cu sites in nabokoite are isolated from each other, and instead of $Te^{4+}O_3$ trigonal pyramids, nabokoite contains perfect tetragonal $Te^{4+}O_4$ pyramids (Pertlik and Zemann, 1988).

Eztlite may be related to cuzticite (reported formula $Fe_2^{3+}Te^{6+}O_6{\cdot}3H_2O$), which was first described in the same paper as eztlite, and is noted to sometimes occur in close proximity to eztlite (Williams, 1982). Cuzticite is also being studied currently by the authors to determine its elemental composition and structure.

As discussed above, eztlite displays far more similarity to minerals with a mitridatite-like structure (Huminicki and Hawthorne, 2002, Moore and Araki, 1977) than to any known Te oxysalt structures.

Acknowledgements

This study has been partly funded by The Ian Potter Foundation grant 'tracking tellurium' to SJM and a Museums Victoria 1854 Student Scholarship awarded to OPM, which we gratefully acknowledge. The single-crystal work was undertaken using the MX2 beamline at the Australian Synchrotron, part of ANSTO, and made use of the Australian Cancer Research Foundation (ACRF) detector. Microprobe work was funded through Natural Environment Research Council grant NE/M010848/1 'Tellurium and Selenium Cycling and Supply' to Chris J. Stanley (Natural History Museum, London). The picture of eztlite on specimen M54056 (Fig. 1) was taken with the assistance of David Paul (Museums Victoria, Australia).

Associate Editor Ferdinando Bosi, and three reviewers (Peter Leverett, Anthony Kampf and one anonymous reviewer) are thanked for their comments and suggestions which improved the manuscript and reported crystal structure.

Supplementary material

To view supplementary material for this article, please visit https://doi.org/10.1180/mgm.2018.108

References

Andrade, M.B., Morrison, S.M., Di Domizio, A.J., Feinglos, M.N. and Downs, R.T. (2012) Robertsite, $Ca_2Mn_3^{III}O_2(PO_4)_3{\cdot}3H_2O$. *Acta Crystallographica*, **E68**, i74–i75.

Brese, N.E. and O'Keeffe, M. (1991) Bond-valence parameters for solids. *Acta Crystallographica*, **B47**, 192–197.

Bruker (2001) *SADABS and XPREP*. Bruker AXS Inc., Madison, WI, USA.

Burns, P.C., Pluth, J.J., Smith, J.V., Eng, P., Steele, I. and Housley, R.M. (2000) Quetzalcoatlite: a new octahedral-tetrahedral structure from a $2{\times}2{\times}40\ \mu m^3$ crystal at the Advanced Photon Source-GSE-CARS facility. *American Mineralogist*, **85**, 604–607.

Christy, A.G. and Mills, S.J. (2013) Effect of lone-pair stereoactivity on polyhedral volume and structural flexibility: application to $Te^{IV}O_6$ octahedra. *Acta Crystallographica*, **B69**, 446–456.

Christy, A.G., Mills, S.J. and Kampf, A.R. (2016) A review of the structural architecture of tellurium oxycompounds. *Mineralogical Magazine*, **80**, 415–545.

Degen, T., Sadki, M., Bron, E., König, U. and Nénert, G. (2014) The Highscore suite. *Powder Diffraction*, **29**, S13–S18.

Effenberger, H., Zemann, J. and Mayer, H. (1978) Carlfriesite; crystal structure, revision of chemical formula, and synthesis. *American Mineralogist*, **63**, 847–852.

Feger, C.R., Kolis, J.W., Gorny, K. and Pennington, C. (1999) Rodalquilarite revisited: the hydrothermal synthesis and structural reinvestigation of $H_3Fe_2(TeO_3)_4Cl$. *Journal of Solid State Chemistry*, **143**, 254–259.

Gagné, O.C. and Hawthorne, F.C. (2015) Comprehensive derivation of bond-valence parameters for ion pairs involving oxygen. *Acta Crystallographica*, **B71**, 562–578.

Huminicki, D.M.C. and Hawthorne, F.C. (2002) The crystal chemistry of phosphate minerals. Pp. 123–253 in: *Phosphates – Geochemical, Geobiological and Materials Importance* (M.L. Kohn, J. Rakovan and J. M. Hughes, editors). Reviews in Mineralogy & Geochemistry, **48**. Mineralogical Society of America and the Geochemical Society, Washington, DC.

Kabsch, W. (2010). XDS. *Acta Crystallographica*, **D66**, 125–132.

Kampf, A.R. and Mills, S.J. (2011) The role of hydrogen in tellurites: crystal structure refinements of juabite, poughite and rodalquilarite. *Journal of Geosciences*, **56**, 235–247.

Kampf, A.R., Mills, S.J. and Rumsey, M.S. (2017) The discreditation of girdite. *Mineralogical Magazine*, **81**, 1125–1128.

Kraus, W. and Nolze, G. (1996) POWDER CELL – a program for the representation and manipulation of crystal structures and calculation of the resulting X-ray powder patterns. *Journal of Applied Crystallography*, **29**, 301–303.

Krivovichev, S.V. and Brown, I.D. (2001) Are the compressive effects of encapsulation an artifact of the bond valence parameters? *Zeitschrift für Kristallographie*, **216**, 245–247.

Laugier, J. and Bochu, B. (2004) Chekcell: Graphical powder indexing cell and space group assignment software, http://www.ccp14.ac.uk/tutorial/lmgp/.

Mills, S.J. and Christy, A.G. (2013) Revised values of the bond-valence parameters for Te^{IV}–O, Te^{VI}–O and Te^{IV}–Cl. *Acta Crystallographica*, **B69**, 145–149.

Moore, P. and Ito, J. (1974) Isotypy of robertsite, mitridatite, and arseniosiderite. *American Mineralogist*, **59**, 48–59.

Moore, P.B. and Araki, T. (1977) Mitridatite, $Ca_6(H_2O)_6[Fe_9^{3+}O_6(PO_4)_9]\cdot 3H_2O$. A noteworthy octahedral sheet structure. *Inorganic Chemistry*, **16**, 1096–1106.

Pasero, M. (2017) The New IMA List of Minerals, http://nrmima.nrm.se/.

Pertlik, F. and Zemann, J. (1988) The crystal structure of nabokoite, $Cu_7TeO_4(SO_4)_5\cdot KCl$: The first example of a $Te^{(IV)}O_4$ pyramid with exactly tetragonal symmetry. *Mineralogy and Petrology*, **38**, 291–298.

Pouchou, J.L. and Pichoir, F. (1991) Quantitative analysis of homogeneous or stratified microvolumes applying the model "PAP". Pp. 31–75 in: *Electron Probe Quantification*, (K.F.J. Heinrich and D.E. Newbury, editors). Plenum Press, New York.

Roberts, A.C., Gault, R.A., Jensen, M.C., Criddle, A.J. and Moffatt, E.A. (1997) Juabite, $Cu_5(Te^{6+}O_4)_2(As^{5+}O_4)_2\cdot 3H_2O$, a new mineral species from the Centennial Eureka mine, Juab County, Utah. *Mineralogical Magazine*, **61**, 139–144.

Sheldrick, G.M. (2015*a*) SHELXT – Integrated space-group and crystal-structure determination. *Acta Crystallographica*, **A71**, 3–8.

Sheldrick, G.M. (2015*b*) Crystal structure refinement with SHELXL. *Acta Crystallographica*, **C71**, 3–8.

Voloshin, A., Men'shikov, Y.P., Polezhaeva, L. and Lentsi, A. (1982) Kolfanite, a new mineral from granite pegmatite, Kola Peninsula. *Mineralogicheskiy Zhurnal*, **4**, 90–95.

Williams, S.A. (1982) Cuzticite and eztlite, two new tellurium minerals from Moctezuma, Mexico. *Mineralogical Magazine*, **46**, 257–259.